16 State House Station
Augusta, Maine 04333

Transportation Research Division

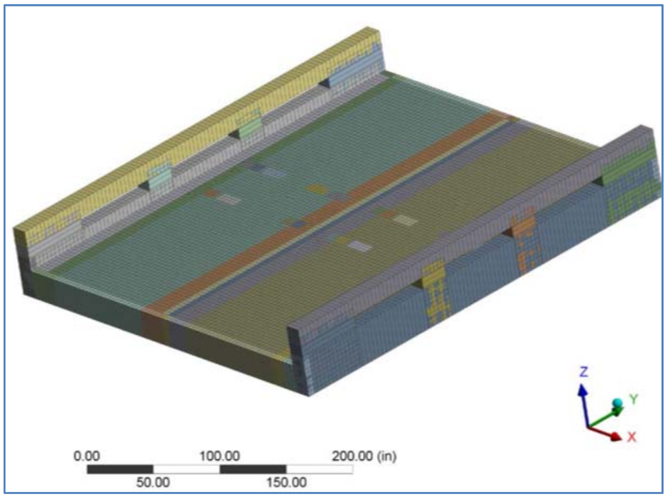

Technical Report 17-06

Advanced Bridge Safety Initiative: Phase 2

Task 2

Effects of Curb and Railing Inclusion on Rating Factors of Reinforced Concrete Flat Slab Bridges Using Finite Element Analysis

March 2017

Technical Report Documentation Page

1. Report No.	2.	3. Recipient's Accession No.	
ME 17-06			
4. Title and Subtitle Advanced Bridge Safety Initiative: Phase 2, Task 2 - Effects of Curb and Railing Inclusion on Rating Factors of Reinforced Concrete Flat Slab Bridges Using Finite Element Analysis		5. Report Date March 2017	
		6.	
7. Author(s) Scott Tomlinson P.E., William Davids Ph.D, P.E. Andrew Schanck, Undergraduate Research Assistant		8. Performing Organization Report No. 16-22-1332.2	
9. Performing Organization Name and Address Advanced Structures and Composites Center University Of Maine 35 Flagstaff Rd. Orono, ME 04469		10. Project/Task/Work Unit No. Project 017666.00	
		11. Contract © or Grant (G) No. Contract # 20160617*4564	
12. Sponsoring Organization Name and Address Maine Department of Transportation		13. Type of Report and Period Covered	
		14. Sponsoring Agency Code	
15. Supplementary Notes			
16. Abstract (Limit 200 words)			

The Maine Department of Transportation (Maine DOT) owns a number of existing reinforced concrete slab bridges that utilize the standard Maine concrete bridge rail. At issue is the additional stiffening and strengthening that the curb and this rail provides to these structures, especially at the slab edge which is often the critical location for load rating. The University of Maine (UMaine) conducted finite-element parametric studies to assess the effect of the integral curb and integral bridge rail on slab capacity as measured by the HL-93 inventory rating factor (RF). The analyses focused on typical, two-lane slab bridges. Overall, it was found that incorporating the stiffness of the integrated thickened curb increased the rating factor for concrete flat slab bridges from 1.0 to between 1.24 and 1.73 depending upon span and whether or not a wearing surface (WS) was included. When the stiffness of the integrated curb and rail was included in the analysis the rating factor increased from 1.0 to at least 1.90 depending on span and wearing surface inclusion.

17. Document Analysis/Descriptors		18. Availability Statement	
Bridge load rating, reinforced concrete slab, finite element analysis			
19. Security Class (this report)	20. Security Class (this page)	21. No. of Pages	22. Price
		21	

Effects of Curb and Railing Inclusion on Rating Factors of Reinforced Concrete Flat Slab Bridges Using Finite Element Analysis

Prepared for:
Dale Peabody P.E.
Director Transportation Research
Maine Dept. of Transportation
16 State House Station
Augusta ME 04333-0016
University of Maine's Advanced Structures and Composites Center
Report Number: 16-22-1332.2

2017-03-31-Rev00

Prepared by:
Scott Tomlinson, PE, SCWI, Research Engineer
Andrew Schanck, Undergraduate Research Assistant

William Davids, PhD, PE
John C. Bridge Professor of Civil and Environmental Engineering

Reviewed by:
Joshua Clapp, PE
Research Engineer

Advanced Structures and Composites Center
35 Flagstaff Rd
University of Maine
Orono, ME 04469

Telephone: 207-581-2123
FAX: 207-581-2074
composites@maine.edu
www.composites.umaine.edu

Document Log

Name/ Organization	Date	Version	Action
Scott Tomlinson, Author Andrew Schanck, Author William Davids, Author Joshua Clapp, Reviewer	2017-03-31	Rev00	Initial release to MaineDOT.

Table of Contents

Index of Figures

Index of Tables

Acronyms

Cases

AASHTO : American Association of Sate Highway and Transportation Officials ... 5
Maine DOT : Maine Department of Transportation ... 4
RC: Reinforced Concrete ... 5
RF: Rating Factor ... 4
UMaine: The University of Maine ... 4
WS: Wearing Surface ... 4

Executive Summary

The Maine Department of Transportation (Maine DOT) owns a number of existing reinforced concrete slab bridges that utilize the standard Maine concrete bridge rail. At issue is the additional stiffening and strengthening that the curb and this rail provides to these structures, especially at the slab edge which is often the critical location for load rating. The University of Maine (UMaine) conducted finite-element parametric studies to assess the effect of the integral curb and integral bridge rail on slab capacity as measured by the HL-93 inventory rating factor (*RF*). The analyses focused on typical, two-lane slab bridges. Overall, it was found that incorporating the stiffness of the integrated thickened curb increased the rating factor for concrete flat slab bridges from 1.0 to between 1.24 and 1.73 depending upon span and whether or not a wearing surface (WS) was included. When the stiffness of the integrated curb and rail was included in the analysis the rating factor increased from 1.0 to at least 1.90 depending on span and wearing surface inclusion. Figure 1 shows the results of the rating factor increase for the integrated curb (left), and integrated curb and railing (right). Table 1 presents a summary of the rating factors calculated for the spans and wearing surface conditions studied.

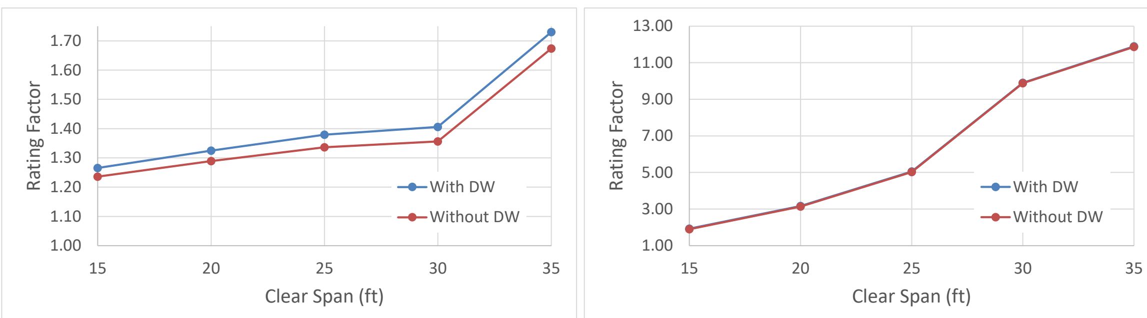

Figure 1: Rating factor increase with incorporation of: integral curb (left), and integral curb with rail (right)

Table 1: Summary of predicted increase in HL-93 inventory rating factors

	With Curb		With Curb and Railing	
Clear Span (ft)	**With WS**	**Without WS**	**With WS**	**Without WS**
15	1.27	1.24	1.92	1.90
20	1.33	1.29	3.17	3.14
25	1.38	1.34	5.05	5.02
30	1.41	1.36	9.90	9.88
35	1.73	1.67	11.89	11.87

1 Background

A review of the literature was performed in order to assess the current state of research into the apparent conservatism inherent in load ratings of RC slab and slab-on-beam bridges produced using American Association of State Highway and Transportation Officials (AASHTO) (2011) (AASHTO, 2011 with 2015 Interim Revisions), the contribution of secondary members to a bridge's structural response to loading, as well as methods of modeling reinforced concrete slabs using finite element methods.

1.1 Conservatism in AASHTO Rating Factors

Numerous studies have indicated that the bridge load rating procedure of equivalent strip analysis for concrete slab bridges described by AASHTO (2011) is often overly conservative (AASHTO, 2011 with 2015 Interim Revisions; Azizinamini et al., 1994b; Azizinamini et al., 1994a; Amer et al., 1999; Jauregui et al., 2007; Jauregui et al., 2010; Kim et al., 2009). This can lead to unnecessary restriction, repair, replacement, or decommissioning of structurally sufficient bridges, including reinforced concrete (RC) slab bridges. In fact, Saraf (1998), using a combination of experimental live-load testing and finite element modeling, found that actual load rating factors could be increased by as much as 110% for RC slab bridges when compared to AASHTO ratings. Mabsout et al. (2004) performed a finite element analysis sensitivity study which varied bridge properties and loading configurations. It was found that AASHTO overestimated edge-beam moment by up to 20% and maximum moment by up to 30% for short span, single lane bridges and underestimated maximum moment by up to 25% for longer, multiple-lane spans. Davids et al. (2013) and Poulin (2012) describe the finite element software, *SlabRate*, purpose designed for the rating of RC slab bridges. Using this program, *RF*'s for 14 RC slab bridges were increased by an average of 24% for unskewed bridges and increased with skew angle up to 300% for bridges with 45° skew. In order to identify some of the factors leading to the apparent discrepancies between AASHTO ratings and true ratings, Chajes and Shenton III (2005) describe a method by which to perform routine diagnostic tests of road bridges, as well as identify information that can be gained from these tests that cannot be determined from AASHTO rating procedures, including detailed girder distribution, support fixity, and stiffness contribution from secondary, nonstructural members.

1.2 Secondary Element Contributions to Rating Factors

One of the major factors which leads to the wide discrepancies between rating factors using AASHTO methodology and those produced from experimental and analytical studies is AASHTO's neglect of the effects of secondary members such as parapets, curbs, sidewalks, and railings (Sanayei et al., 2012; Roddenberry et al., 2011). Smith and Milkelsteins (1988) used grillage analysis to quantify the edge-stiffening characteristics of secondary elements. They found that when incorporated into the analysis, secondary elements could help increase moment capacity and decrease edge beam deflection by 30 and 17% for slab-on-prestressed concrete girders and slab-on-steel girder bridges, respectively. Conner and Huo (2006) investigated the effect of secondary members on distribution factors. They found that the presence of parapets could reduce distribution factors to exterior and interior girders by as much as 36 and 13%, respectively. Eamon and Nowak (2002); (2005) investigated the contribution of secondary elements to bridges' ultimate capacity, girder distribution, and reliability. Through the use of finite element modeling, they determined that the presence of secondary elements increased ultimate capacity from between 110 to 220% and decreased girder distribution factors 10 and 40%. Akinci et al. (2008) performed a finite element analysis to investigate the contribution of secondary members to a bridge's ability to carry loads in excess of its normal operating limit, so-called "super-loads". They found that the presence of secondary members yielded girder distribution factors which could be reduced by up to 30%, allowing greater super-loads to be permitted.

2 Reinforced Concrete Slab Finite Element Modeling

Finite element modeling was conducted on reinforced concrete slab bridges over five representative span lengths using ANSYS Release 17.0 commercial finite element software (ANSYS Mechanical Products, 2015a). These analyses were conducted with three geometries and two wearing surface conditions giving six total models for each bridge length. The three geometries consisted of a plain flat slab, a flat slab with integrated thickened structural curbs, and a flat slab with integrated thickened structural curb and rail. The two wearing surface conditions considered were two inches of bituminous wearing surface and no wearing surface.

Due to its highly complex and non-uniform nature, researchers have suggested many differing finite element approaches to modeling reinforced concrete (RC) slabs ranging from simple linear options to highly complex three dimensional solid non-linear versions (Lewinski and Wojewodzki, 1991; Liu and Teng, 2008; Jiang and Mirza, 1997). The approach taken for this study was to use a simple linearly elastic analysis described in more detail below. A linearly elastic analysis is generally conservative for the most heavily loaded regions of the slab. Since nonlinear behavior, cracking, in those heavily regions would result stress redistribution, lowering the maximum stress relative to the capacity, conducting a linear elastic anlaysis ignoring cracking is a conservative assumption. Further, live load testing of six flat slab bridges in Maine (Davids et al., 2013; Davids and Tomlinson, 2016) has indicated minimal to no slab cracking under truck loads producing approximately 70% of HL-93 load plus impact.

2.1 Geometry

Analyses assume two-lane, simple span bridges with a 24' roadway width. It should be noted here that many slab bridges have a 22' roadway width, but using a larger value corresponding to a modern 12' lane width conservatively reduces the overall stiffening effect of the standard Maine bridge rail, see Appendix A.2. The curb to which the rail is mounted is fixed at 13 inches wide to match the standard rail width, and curb height is fixed at 10 inches based on the lower end of typical values for existing slab bridges previously load rated by UMaine. To be consistent with observed response in prior testing of bridges that are similar to the 14 slab bridges investigated as part of this study, this modeled curb is assumed to be integral with the slab. Additionally, based on Maine Standard Rail details and shear results from the modeling there is sufficient reinforcement between the rail and curb to transfer shear loads so this is modeled as integral as well. Five different overall bridge clear span lengths of 15, 20, 25, 30, and 35 feet are considered based on the analysis of sample RC slab bridges in Maine. Details of this investigation are shown in Appendix A.1. Rail post clear spacing is varied to fit each span, and kept at or below 7'-0", the maximum value allowed per the MaineDOT standard railing detail. Vertical post cross sections are taken as 13"x24" and horizontal cross sections are taken as 14"x13". The standard rail termination length of 4.67' is assumed at each end. Bridge clear spans are taken as one foot less than the overall bridge lengths. A slab span to depth ratio of 18 is maintained through the bridge geometries. This value coincides well with the mean value seen in the sample Maine bridges investigated and summarized in Appendix A.1.

2.2 Boundary Conditions

Simple span conditions were used for all analyses and a sample mesh is shown in Figure 2. Vertical displacements along a line at the ends of the clear spans were fixed to zero with the remaining 6" on each end of the total span overhanging as shown in Figure 3. Horizontal constraints on x translation and y translation were enforced at points shown in Figure 4 and Figure 5 respectively to prevent rigid-body motion of the slabs.

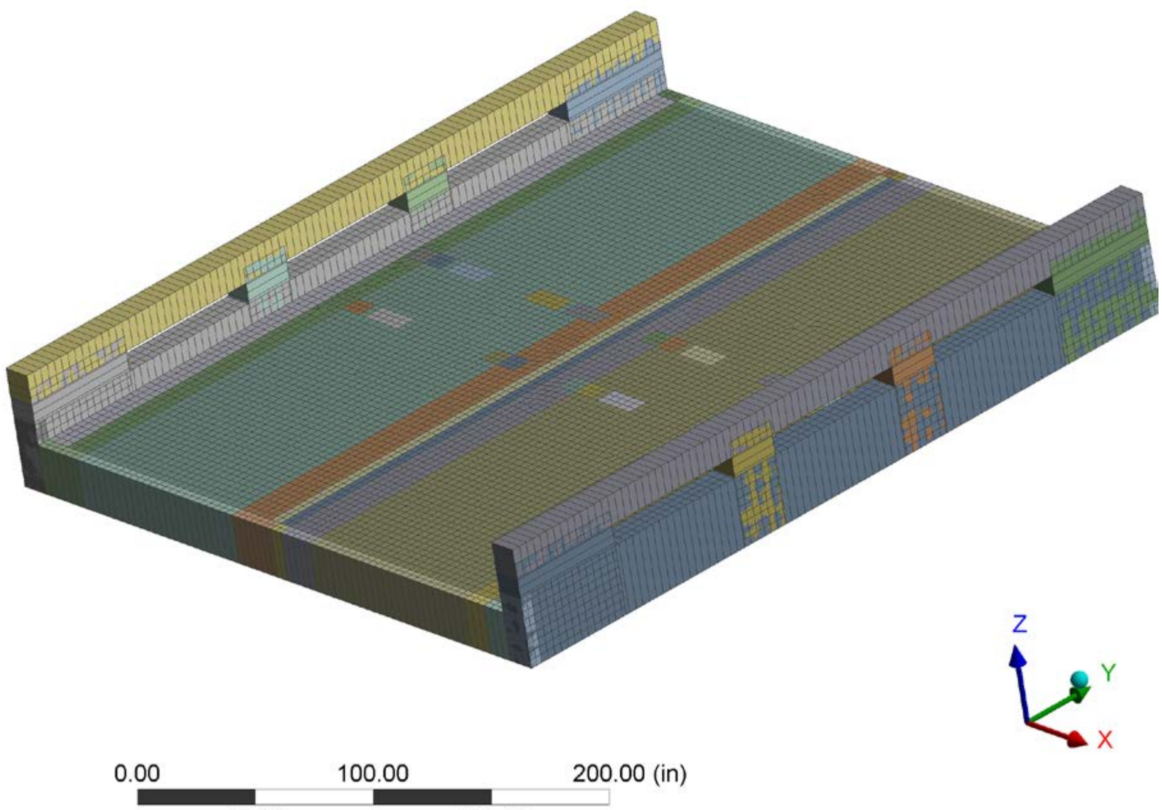

Figure 2: SWR360: Sample Mesh

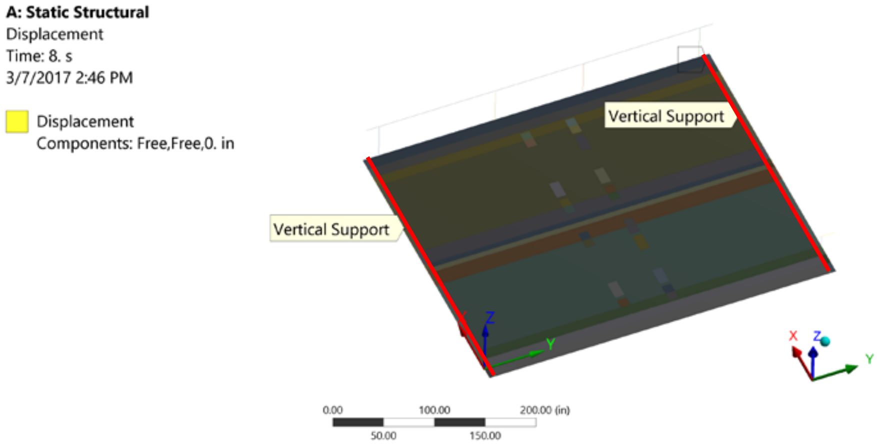

Figure 3: SWR360: Z Boundary Condition (2 Lines)

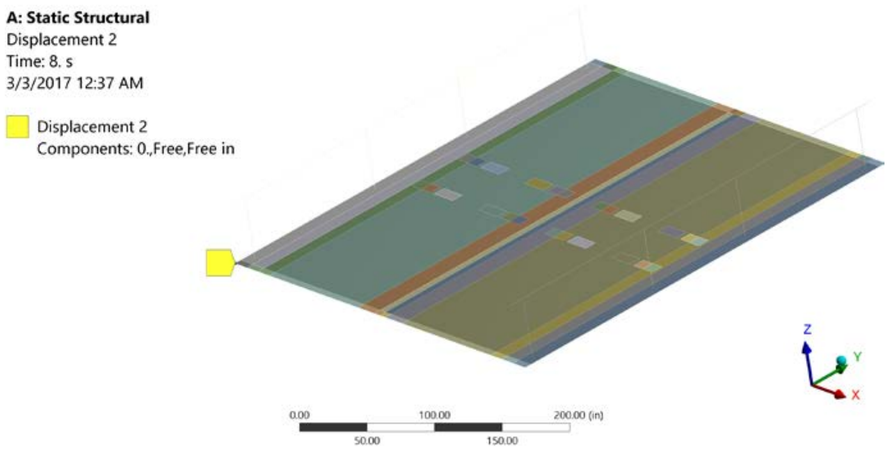

Figure 4: SWR360: *X* Boundary Condition (1 Point)

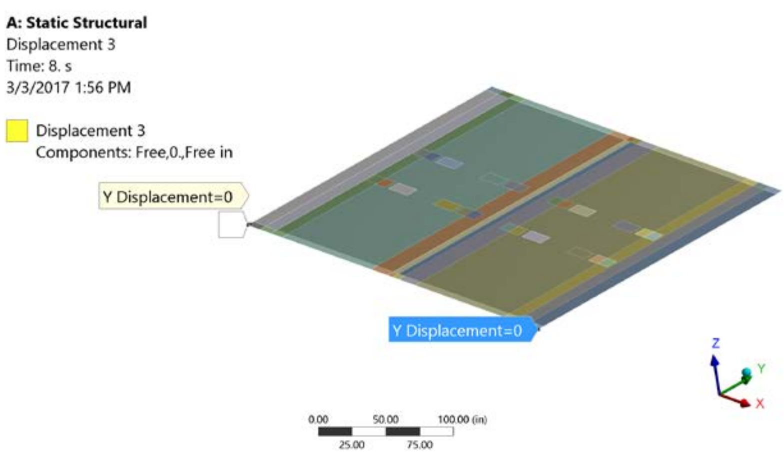

Figure 5: SWR360: *Y* Boundary Condition (2 Points)

2.3 Materials

A linearly elastic isotropic material model was used for the concrete with a density of 150 lbm/ft^3, an elastic modulus of 4.35*10^6 psi, and a Poisson's ratio of 0.2.

2.4 Elements

Two types of elements were used in this study: a shell element for the slab and curb, and a beam element for the rail. The shell element chosen for this study is SHELL281, the same as that used by Poulin (2012) in his study verifying the SlabRate software. SHELL281 is an 8-noded shell element with six degrees of freedom at each node. It uses quadratic shape functions, allows for distribution and load effects of distributed pressures which are used to model the loads, includes the effects of transverse shear, and is suitable for analyzing thin to moderately-thick shell structures (ANSYS Mechanical Products, 2015f). An offset is specified that locates the bottom of all elements at the same elevation when curbs are modeled with integral thickened shell elements. The rails are modeled as BEAM189 elements, which are quadratic 3-D 3-noded beam elements with six degrees of freedom at each node. These elements are compatible with the quadratic shells used for the deck and curb, incorporate Timoshenko beam theory to include shear deformations, and are suitable for analyzing slender to moderately stubby/thick beam structures (ANSYS Mechanical Products, 2015b).

The slab is divided into areas for specific loading areas including lane loads, tandem wheel loads, and curb/railing loads. These areas are modeled as a single slab through the use of contact/ target elements, with CONTA174 contact elements and TARGE170 elements used in conjunction for these slab-slab connections. This pairing between CONTA174, which is specifically designed for 3-D 8 noded surface to surface contact works well for the SHELL281 3-D 8-noded shell elements, and pairs with the TARGE170 element, which is specialized for 3-D deformable target elements (ANSYS Mechanical Products, 2015c; ANSYS Mechanical Products, 2015h). The rail-to-shell connection is fixed in all 6 degrees of freedom and made with CONTA175 elements with TARGE170 elements, where CONTA175 element is a specialized 3-D node to surface contact for the BEAM189 3-D beam to the SHELL281 3-D surface and the TARGE170 element allows for 3-D deformable target elements (ANSYS Mechanical Products, 2015d). The rail-rail connections are fixed in all 6 degrees of freedom and are made with CONTA176 elements with TARGE170 elements, where the CONTA176 is a specialized 3-D line-line contact element and the TARGE170 again allows for deformable 3-D target elements (ANSYS Mechanical Products, 2015e).

2.5 Loads

Loads are applied by SURF154 elements, which allow for complex pressures to be overlaid on an area face of any 3-D element, including the SHELL281 elements used in this study (ANSYS Mechanical Products, 2015g). For plain flat slab models, self-weight of the plain flat slab dead loads are applied as accelerations on the masses of the slab where the acceleration is gravity multiplied by the appropriate factors. This same method is used to model the curb self-weight in the integrated curb model, and the curb with rail in the integrated curb and rail model. Where the curb and rail are not integrated, they are applied as a distributed loads on the slab areas. For the curb this is an exact distribution, for the rail the average load of the rail is taken as the total load of the rail divided by the curb area.

The lane loads and tandem loads are split into west, near *x=0* in the global coordinate system, and east. They are then split into locations within the 12' lane, inner toward the centerline of the bridge, and outer toward the curbs. Each combination of east/west/inner/outer for lane and tandem is multiplied by the appropriate factors – including multiple presence factor, live load factor, and impact factor for the tandem loads – and then is analyzed for load effect. West lane outer is shown in Figure 6, west lane inner is shown in Figure 7, east lane inner is shown in Figure 8, and east lane outer is shown in Figure 9.

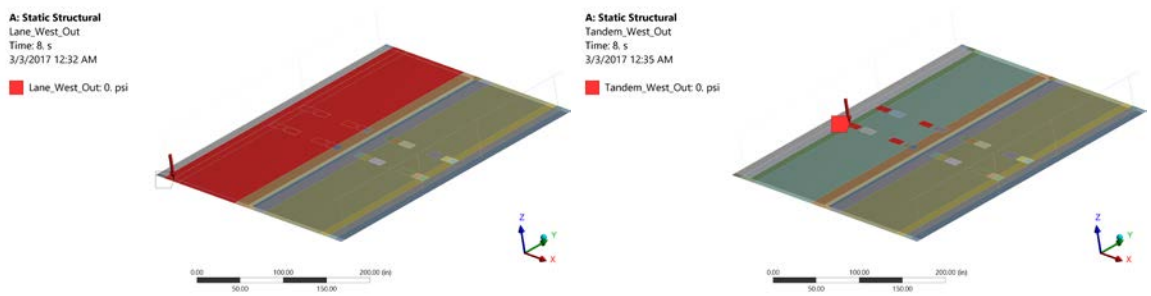

Figure 6: SWR360: Loading, Lane and Tandem, West, Outer

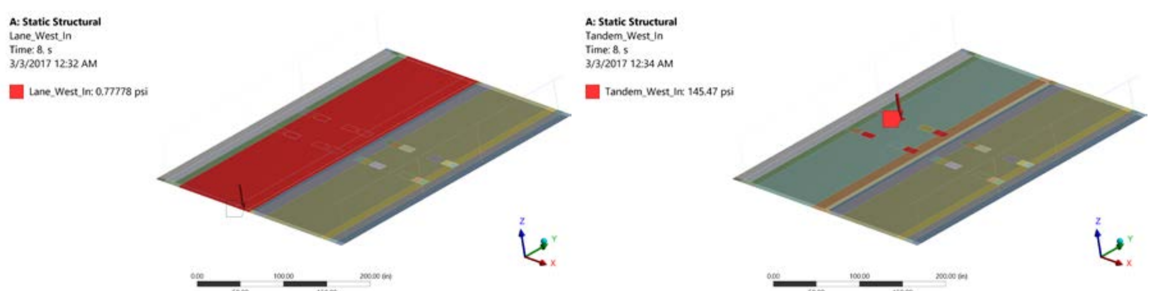

Figure 7: SWR360: Loading, Lane and Tandem, West, Inner

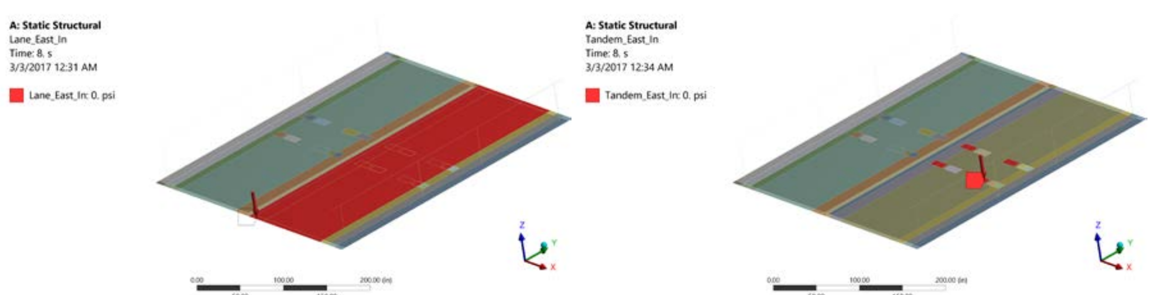

Figure 8: SWR360: Loading, Lane and Tandem, East, Inner

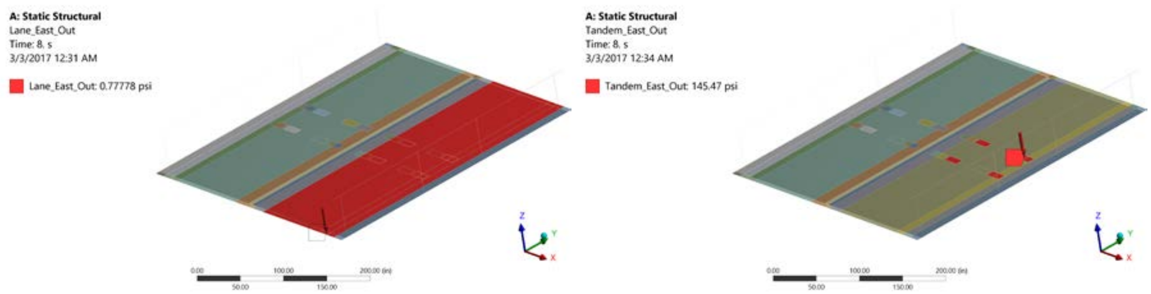

Figure 9: SWR360: Loading, Lane and Tandem, East, Outer

The loading conditions were applied as a time sequence in ANSYS, consisting of 8 steps: dead load self-weight including slab, curb, and rail; dead load wearing surface; one lane west out; one lane west in; two lanes both out; two lanes both in; two lanes west out east in; and two lanes west in east out.

AASHTO (2011 with 2015 Interim Revisions) load factors used are 1.25 for *DC*, 1.50 for *DW*, 1.75 for *LL*, 1+33/100 for *IM*, and a 1.2 multiple presence factor for one lane and 1.0 multiple presence factor for two lanes. The use of the 1.75 *LL* factor is consistent with an inventory rating as opposed to an operating rating which would use a *LL* factor of 1.35. Unfactored loads utilized are 150 lbm/ft^3 for reinforced concrete, 140 lbf/ft^3 for bituminous wearing surface, 25 kip/axle for the tandem load with 20”x10” bearing areas giving 62.5 psi distributed pressure, a lane load of 0.64 kip/ft over a 10’ width giving 0.444 psi, an equivalent curb load of 135.4 lbf/ft, and an equivalent rail load of 154.2 lbf/ft.

2.6 Mesh

A convergence study was performed on the 25’ clear span bridge to determine the maximum element size which could be used. It was determined that a maximum edge length of 4” was adequate to capture stresses in the slab of concern without extreme run times due to overly fine meshes. Figure 10 shows this convergence, with less than 0.23% difference between the finest mesh of 2” and the chosen 4” mesh. A follow-up convergence study was conducted on the 20’ clear span plain flat slab bridge in comparison to the 20’ clear span slab with curb to determine the effect of element size on the final *RF* calculations. Both the plain flat slab and the slab with curb were analyzed with a sequence of refined meshes: 6”, 4”, 2”, and 1”. It was found that the 4” maximum edge length was conservative and predicted a *RF* within 0.07% of that predicted using the smallest mesh size utilized in this study, 1”. Details of the calculation of the *RF* are given later in this report. Figure 11 shows the convergence of the *RF* over maximum element face size. The ANSYS auto-meshing algorithm utilizes many elements of smaller size, but this parameter sets the overall maximum face allowed. A sample of the chosen 4” mesh of both slab and beam elements can be seen in Figure 2.

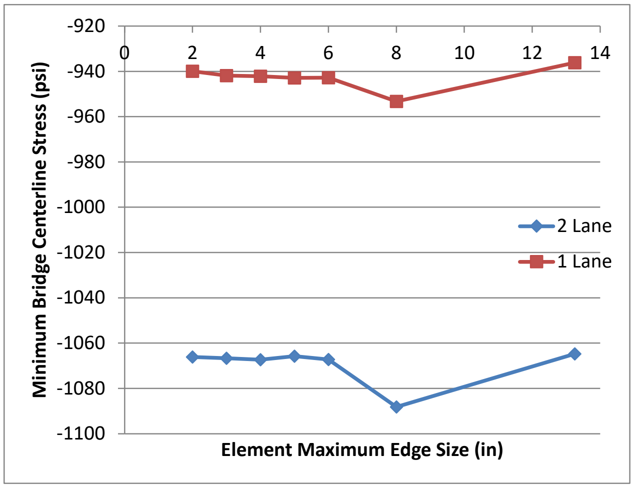

Figure 10: Element convergence

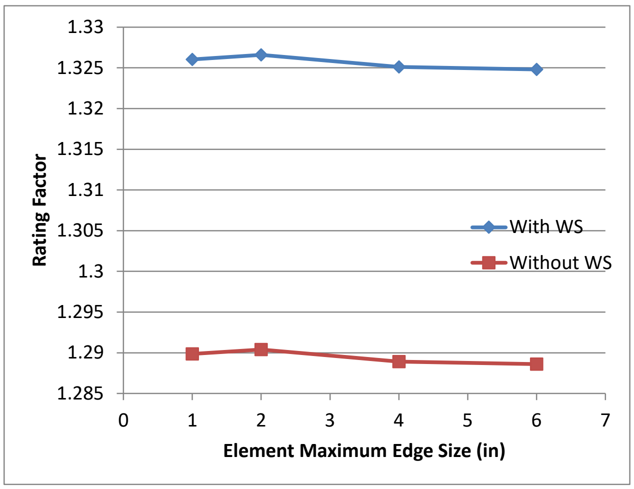

Figure 11: Rating Factor convergence for 20' clear span slab with curb

2.7 Model Verification

Verification of the model was achieved in several ways. The first approach was to calculate the bridge mass analytically and compare equilibrium in the reactions to those of the model. This was verified for each model to be very near 0% error. The second check was to calculate the total moment due to live and dead load across the center of the bridge. This was verified to be within 3% for each plain flat slab and slab with curb model for each dead and live load case prior to investigating the moment distributions across the bridge. A third verification was to compare each plain flat slab model with the results of the previously validated *SlabRate* software (Davids et al., 2013) and verify that the results matched before moving to the more complicated integrated curb and integrated curb with rail models. A fourth verification was to visually check the deflection of the bridge at each step and verify that the deflected shape matched the expected shape based on curb and/or rail inclusion, and load placement. The overall magnitude of relative displacements under relative loads in each step was checked. A fifth check was to verify that the stresses in the top and bottom of the slab were consistent with what was expected based on loading, and also to verify a cross-section of the bridge at the centerline matched the expected distribution with no major variances, as shown in Figure 12. An example of a deflected shape is shown in Figure 13 and an example of the S_y stresses are shown in Figure 14.

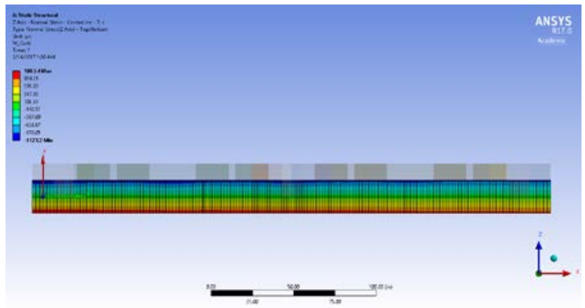

Figure 12: PFS360: Normal forces in the center cross section with 2 lanes of loading shifted to the west (left)

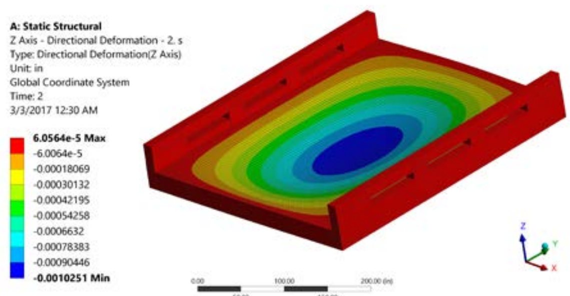

Figure 13: SWR360: Deflection under wearing surface loading

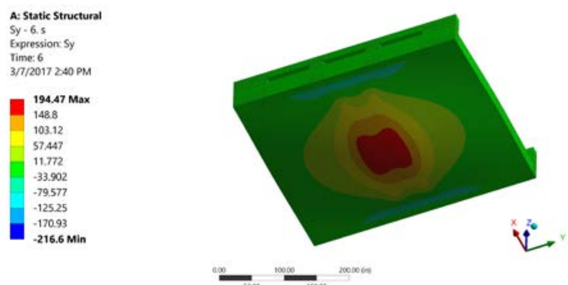

Figure 14: SWR360: S_y bottom of the slab under two lane tandem loading centered and shifted Inner-Inner

3 Finite Element Modeling Rating Factor Methodology

The bridge rating factors are calculated according to Equation 1.

$$RF = \frac{C - \gamma_{DC}DC - \gamma_{DW}DW \pm \gamma_P P}{\gamma_{LL}(LL + IM)} \qquad \text{Equation 1}$$

$C = Value\ producing\ RF = 1.0\ for\ a\ plain\ flat\ slab$

$\gamma_{DC} = 1.25$ per Table 6A.4.2.2-1

$\gamma_{DW} = 1.50$ per Table 6A.4.2.2-1

$\gamma_{LL} = 1.75$ per Table 6A.4.2.2-1

$P = 0$ for all bridges in this study

Each configuration of geometry was first analyzed as a plain flat slab under all loading cases, and the critical controlling loading case was determined based on the highest imparted moment in the slab. The capacity *C* was then calculated to produce an *RF* of 1.0, and the analyzed *DC*, *DW*, and *LL+IM* for selected strips in the slab. The bridge was then analyzed with integrated curbs, and the new rating factor was calculated using the now known capacity, and new values of *DC*, *DW*, and *LL+IM* moment. The same procedure was repeated for models with the integrated curb and rail.

The moment within the slab was calculated as the average over each element. The top and bottom cross section stresses for each element were assumed to vary linearly and used to integrate the stress over the depth of the element to determine the moment according to Equation 2. This method is described by Cook et al. (2002) and a similar method was used by Poulin (2012) in the verification of the *SlabRate* software.

$$M_y = \int_{-t/2}^{t/2} \sigma_y z \, dz \qquad \text{Equation 2}$$

$M_y = bending\ moment\ per\ unit\ length$

$t = thickness\ of\ slab$

$z = distance\ from\ midsurface$

$\sigma_y = cross\ section\ stress$

For all plain flat slab bridges the load case of two tandem trucks shifted to one side of the bridge caused the maximum observed moment in the slab occurring at the slab edge. Figure 15 shows the longitudinal stress in the bottom of the slab for the 240” clear span plain flat slab bridge, with the element with maximum moment observed labeled as well as the values of the stresses with maximum noted. For all slab with curb and slab with curb and railing the worst case moment occurred very near the center middle of the bridge, in all cases with the worst case loading as two tandems shifted as far toward the middle as allowed by AASHTO. Figure 16 shows the longitudinal stress in the bottom of the slab for the 240” clear span plain flat slab bridge, with the element with maximum moment observed labeled as well as the values of the stresses with the maximum noted. The slabs span in the *y*-direction.

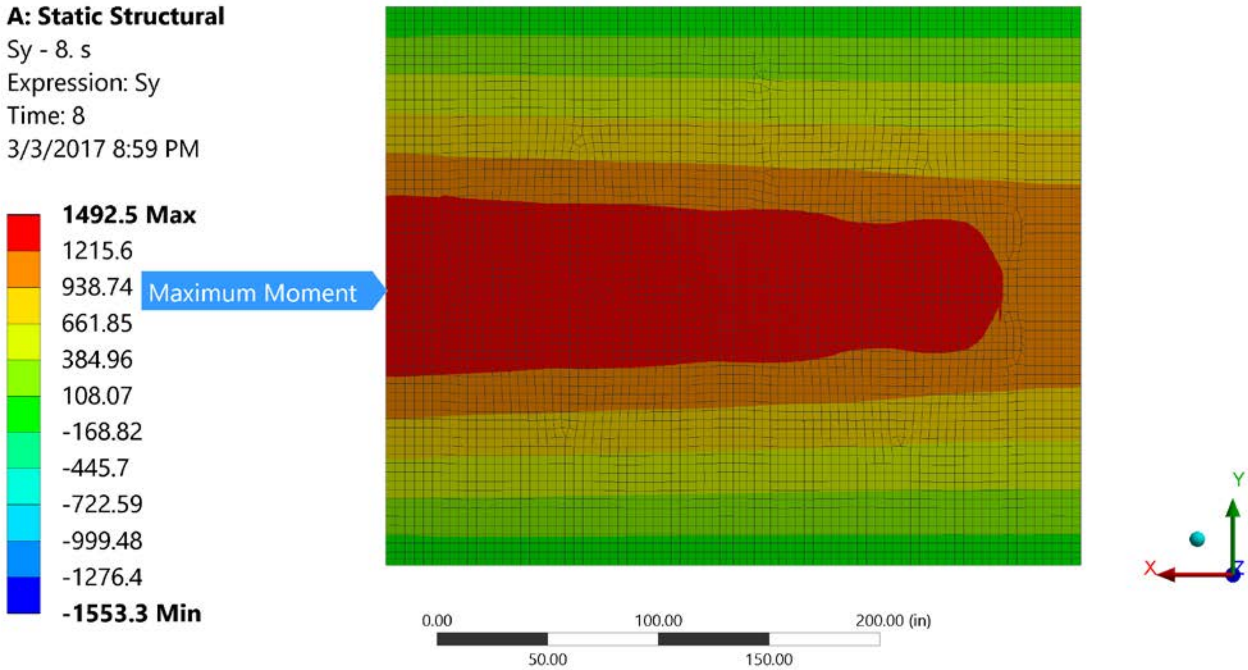

Figure 15: Plain flat slab (No curb) 240” clear S_y Bottom of slab: maximum moment location

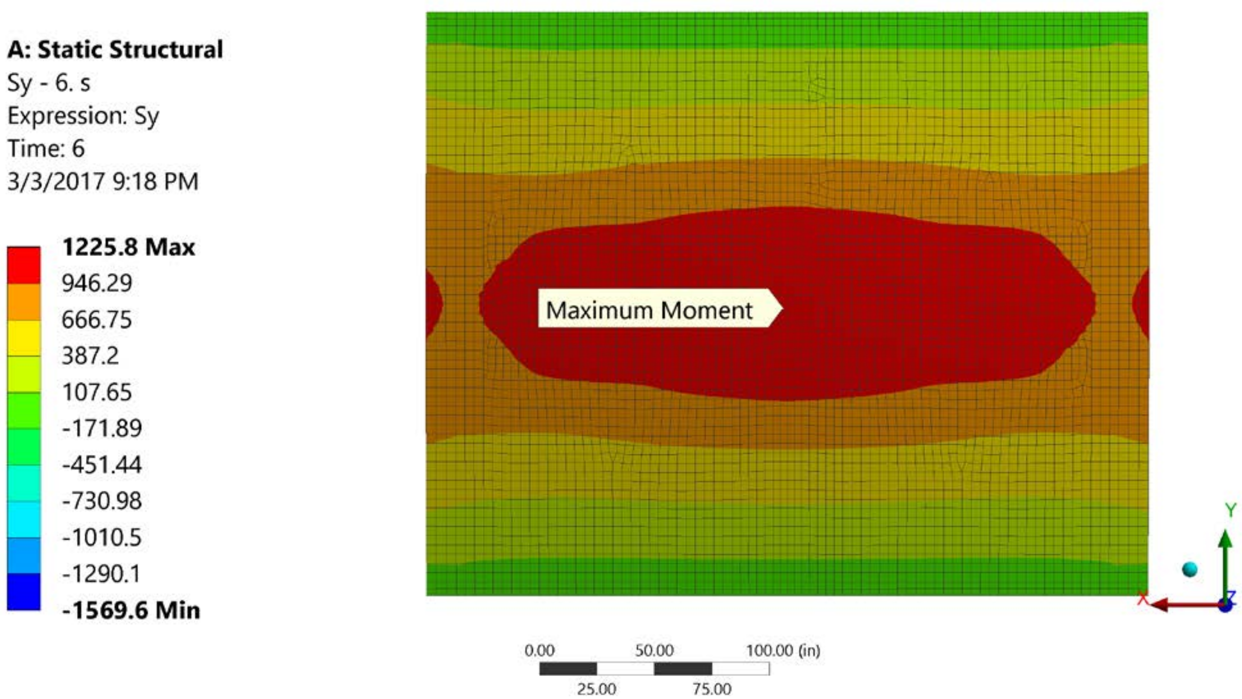

Figure 16: Slab with Curb 240" clear Sy Bottom of Slab: maximum moment location

4 Summary of Analyses and Conclusions

Overall, the rating factors were shown to be conservative when analyzing the plain flat slab without any integrated curb or rail. The most defensible and reliable increase in rating factor is that due to the integral curb without the railing. In most bridges, the curbs and slab are placed at the same time, and reinforcement details are likely to be accurate. The integral curb provides *RF* increases of between 1.24 and 1.73 relative to an initial rating factor of 1.0, with increasing *RF* with increasing span length. The increase in *RF* with increasing span length reflects the bridge acting more like a single unit with more uniform bending across the slab width as span length increases. The exact values for each span with and without wearing surface, along with a linear least squares regression fit, are provided in Table 2. The linear least squares regression for the *RF* with curb is for span lengths 15' to 30', while the regression fit for curb and rail is from 15' to 35'. The predicted *RF* increase resulting from the integrated curb with railing is likely less reliable than that with curb alone due to the highly variable nature of the construction quality, fit tolerances, and condition of the rail. Any increase in rating factor, whether from integrated curb or integrated curb and rail, should be carefully considered by the bridge owner prior to acceptance.

Table 2: Summary of predicted increases in HL-93 inventory rating factors

	With Curb		With Curb and Railing	
Clear Span (ft)	**With WS**	**Without WS**	**With WS**	**Without WS**
15	1.27	1.24	1.92	1.90
20	1.33	1.29	3.17	3.14
25	1.38	1.34	5.05	5.02
30	1.41	1.36	9.90	9.88
35	1.73	1.67	11.89	11.87
Slope	9.523E-03	8.167E-03	0.533	0.534
Intercept	1.130	1.121	-6.95	-6.98
R^2	0.974	0.965	0.952	0.952

5 References

AASHTO. (2011 with 2015 Interim Revisions) The Manual For Bridge Evaluation Second Edition. Second ed. Washington DC: American Association of State Highway and Transportation Officials.

Akinci N, Liu J and Bowman M. (2008) Parapet Strength and Contribution to Live-Load Response for Superload Passages. *Journal of Bridge Engineering* 13: 55-63.

Amer A, Arockiassmy M and Shahawy M. (1999) Load Distribution of Existing Solid Slab Bridges Based on Field Tests. *Journal of Bridge Engineering* 4: 189-193.

ANSYS Mechanical Products. (2015a). ANSYS, Inc.

ANSYS Mechanical Products. (2015b) Ansys Documentation, Mechanical APDL, Element Reference, Element Library, BEAM189. ANSYS, Inc.

ANSYS Mechanical Products. (2015c) Ansys Documentation, Mechanical APDL, Element Reference, Element Library, CONTA174. ANSYS, Inc.

ANSYS Mechanical Products. (2015d) Ansys Documentation, Mechanical APDL, Element Reference, Element Library, CONTA175. ANSYS, Inc.

ANSYS Mechanical Products. (2015e) Ansys Documentation, Mechanical APDL, Element Reference, Element Library, CONTA176. ANSYS, Inc.

ANSYS Mechanical Products. (2015f) Ansys Documentation, Mechanical APDL, Element Reference, Element Library, SHELL281. ANSYS, Inc.

ANSYS Mechanical Products. (2015g) Ansys Documentation, Mechanical APDL, Element Reference, Element Library, SURF154. ANSYS, Inc.

ANSYS Mechanical Products. (2015h) Ansys Documentation, Mechanical APDL, Element Reference, Element Library, TARGE170. ANSYS, Inc.

Azizinamini A, Boothby T, Shekar Y, et al. (1994a) Old Concrete Slab Bridges. I: Experimental Investigation. *Journal of Structural Engineering* 120: 3284-3304.

Azizinamini A, Shekar Y, Boothby T, et al. (1994b) Old Concrete Slab Bridges. II: Analysis. *Journal of Structural Engineering* 120: 3305-3319.

Chajes M and Shenton III H. (2005) Using Diagnostic Load Tests for Accurate Load Rating of Typical Bridges. *Structures Congress 2005.* New York, NY: ASCE.

Conner S and Huo X. (2006) Influence of Parapets and Aspect Ratio on Live-Load Distribution. *Journal of Bridge Engineering* 11: 188-196.

Cook RD, Malkus DS, Plesha ME, et al. (2002) *Concepts and Applications of FInite Element Analysis,* University of Wisconsin - Madison: John Wiley & Sons, Inc.

Davids W, Poulin T and Goslin K. (2013) Finite-Element Analysis and Load Rating of Flat Slab Concrete Bridges. *Journal of Bridge Engineering* 18: 946-956.

Davids W and Tomlinson S. (2016) Instrumentation During Live Load Testing and Load Rating of Five Reinforced Concrete Slab Bridges Report 16-23-1332.3. The University of Maine Advanced Structures and Composites Center, 44.

Eamon C and Nowak A. (2002) Effects of Edge-Stiffening Elements and Diaphragms on Bridge Resistance and Load Distribution. *Journal of Bridge Engineering* 7: 258-266.

Eamon C and Nowak A. (2005) Effect of Edge Stiffening and Diaphragms on the Reliability of Bridge Girders. *Journal of Bridge Engineering* 10: 206-214.

Jauregui D, Licon-Lozano A and Kulkarni K. (2007) Improved Load Rating of Reinforced Concrete Slab Bridges. In: New Mexico Department of Transportation (ed). Albuquerque, NM: NMDOT.

Jauregui D, Licon-Lozano A and Kulkarni K. (2010) Higher Level Evaluation of a reinforces Concrete Slab Bridge. *Journal of Bridge Engineering* 15: 172-182.

Jiang J and Mirza F. (1997) Nonlinear analysis of reinforced concrete slabs by a discrete finite element approach. *Computers & Structures* 65: 585-592.

Kim Y, Rusmir T and Wright R. (2009) Recent Advances in Performance Evaluation and Flexural Response of Existing Bridges. *Journal of Performance of Constructed Facilities* 23: 190-200.

Lewinski P and Wojewodzki W. (1991) Integrated Finite Element Model for Reinforced Concrete Slabs. *Journal of Structural Engineering* 117: 1017-1038.

Liu Y and Teng S. (2008) Nonlinear Analysis of Reinforced Concrete Slabs Using Nonlayered Shell Element. *Journal of Structural Engineering* 134: 1092-1100.

Mabsout M, Tarhini K, Jabakhanji R, et al. (2004) Wheel Load Distribution in Simply Supported Concrete Slab Bridges. *Journal of Bridge Engineering* 9: 147-155.

Poulin TJ. (2012) Development of Improved Analytical Load Rating Procedures for Flat Slab Concrete Bridges. *Department of Civil and Environmental Engineering.* Orono, ME: The University of Maine.

Roddenberry M, Chipperfield J and Tawfiq K. (2011) Effect of Secondary Elements on Load Distribution in Prestressed Bridge Girders. In: Ames D, Droessier T and Hoit M (eds) *Structures Congress 2011.* Las Vegas, NV: ASCE.

Sanayei M, Phelps J, Sipple J, et al. (2012) Instrumentation, Nondestructive Testing and Finite-Element Model Updating for Bridge Evaluation Using Strain Measurements. *Journal of Bridge Engineering* 17: 130-138.

Saraf V. (1998) Evaluation of Existing RC Slab Bridges. *Journal of Performance of Constructed Facilities* 12: 20-24.

Smith K and Milkelsteins I. (1988) Load Distribution in Edge Stiffened Slab and Slab-on-Girder Bridge Decks. *Canadian Journal of Civil Engineering* 15: 977-983.

A.1 Sample Maine Bridge Configurations

Fourteen reinforced concrete slab bridges were investigated for this study. Analysis was conducted to determine average and standard deviations for clear span and length/depth ratios. Bridge clear spans and span/depth ratios are presented in figures 19 and 20 respectively. The bridges examined are shown in Table 3.

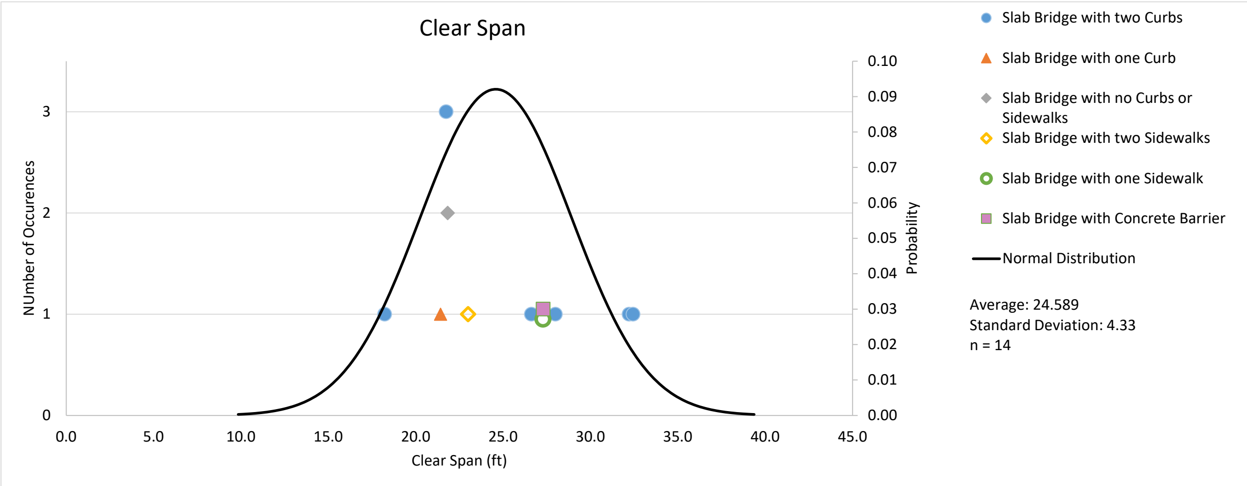

Figure 17: Sample bridge clear spans

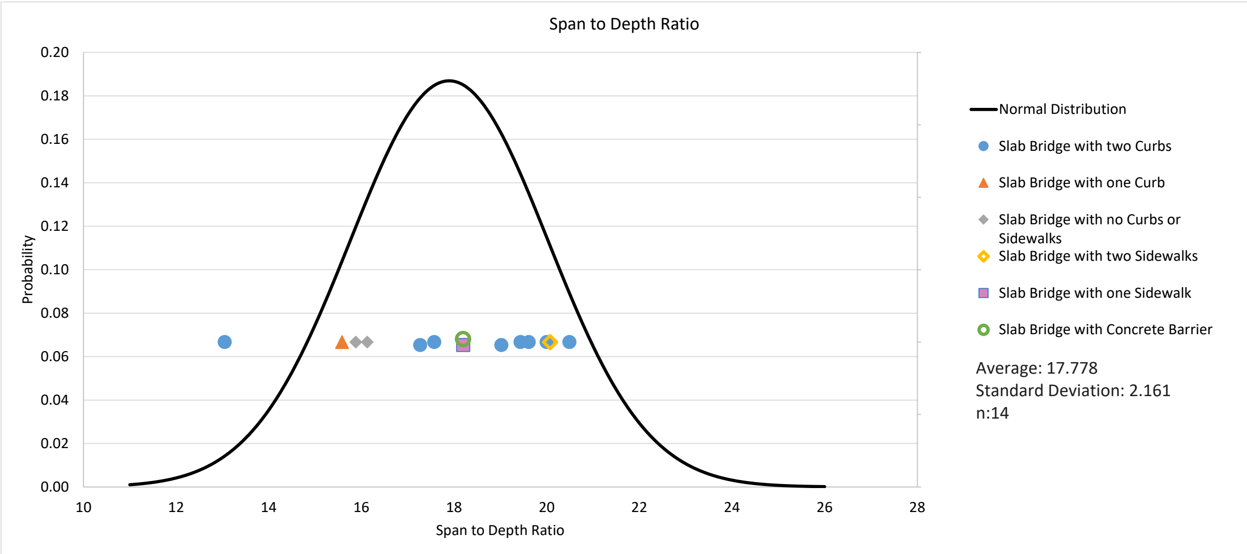

Figure 18: Sample bridge span/depth ratios

Table 3: Sample bridges examined, lengths in (m)

Bridge	Woolwich/ Wiscasset	Weld	Argyle	Carmel	Clinton	Levant	Milford	Palmyra	Paris	Smyrna	Penobscot Hancock County	Brewer	Milo Left Side	Milo Right Side
No.	2577	5361	3827	5191	3579	5253	2070	5699	2582	2250	3297	5638	2931	2931
Clear Span along *cl*	6.629	9.890	6.664	9.820	5.556	8.115	8.382	6.477	6.531	6.655	6.553	7.010	8.321	8.321
Roadway Width	7.315	7.375	7.315	6.706	7.315	6.706	8.534	8.534	6.121	3.566	3.302	8.534	4.686	4.686
Slab Thickness	0.508	0.483	0.343	0.559	0.292	0.470	0.419	0.330	0.419	0.419	0.406	0.349	0.457	0.457
Span/Depth Ratio	13.050	20.493	19.435	17.574	19.022	17.270	20.000	19.615	15.583	15.879	16.125	20.073	18.199	18.199

Notes:

Blue is slab bridge with two curbs
Orange is slab bridge with one curb
Grey is slab bridge with no curbs or sidewalks
Yellow is slab bridge with two sidewalks
Green is slab bridge with one sidewalk
Red is slab bridge with one side concrete barrier

Advanced Structures and Composites Center
35 Flagstaff Rd
University of Maine
Orono, ME 04469

Telephone: 207-581-2123
FAX: 207-581-2074
composites@maine.edu
www.composites.umaine.edu

A.2 Maine Department of Transportation Standard Bridge Railing Detail